Planets in Stellar Clusters Extensive Search. III. A search for transiting planets in the metal-rich open cluster NGC 6791.[1]

B. J. Mochejska[2]
Purdue University, Department of Physics, 525 Northwestern Ave., West Lafayette, IN 47907
bmochejs@cfa.harvard.edu

K. Z. Stanek, D. D. Sasselov, A. H. Szentgyorgyi, G. Á. Bakos[2,3], J. Devor, V. Hradecky, D. P. Marrone, J. N. Winn[2] & M. Zaldarriaga
Harvard-Smithsonian Center for Astrophysics, 60 Garden St., Cambridge, MA 02138
kstanek, sasselov, saint, gbakos, jdevor, vhradecky, dmarrone, jwinn, mzaldarriaga@cfa.harvard.edu

ABSTRACT

We have undertaken a long-term project, Planets in Stellar Clusters Extensive Search (PISCES), to search for transiting planets in open clusters. In this paper we present the results for NGC 6791 – a very old, populous, metal rich cluster. We have monitored the cluster for over 300 hours, spread over 84 nights. We have not detected any good transiting planet candidates. Given the photometric precision and temporal coverage of our observations, and current best estimates for the frequency and radii of short-period planets, the expected number of detectable transiting planets in our sample is 1.5. We have discovered 14 new variable stars in the cluster, most of which are eclipsing binaries, and present high precision light curves, spanning two years, for these new variables and also the previously known variables.

Subject headings: planetary systems – binaries: eclipsing – cataclysmic variables – stars: variables: other – color-magnitude diagrams

1. Introduction

We have undertaken a long-term project, Planets in Stellar Clusters Extensive Search (PISCES), to search for transiting planets in open clusters. To date we have published a feasibility study based on one season of data for NGC 6791 (Mochejska et al. 2002, hereafter Paper I). We have also presented a variable star catalog in our second target, NGC 2158, based on the data from the first observing season (Mochejska et al. 2004, hereafter Paper II).

In this paper we present the results of a search for transiting planets in the open cluster NGC 6791 [$(\alpha,\delta)_{2000} = (19^h20.8^m, +37°51')$]. It is a very populous (Kaluzny & Udalski 1992), very old (τ=8 Gyr), extremely metal rich ([Fe/H]=+0.4) cluster, located at a distance modulus of $(\text{m-M})_V$ = 13.42 (Chaboyer, Green & Liebert 1999).

Stars hosting planets are known to be, on the average, significantly more metal rich than those without (Santos et al. 2001, 2004). Two scenarios have been proposed to explain this phenomenon. Some studies favor a "primordial" metallicity enhancement, i.e. reflecting the original metallicity of the gas from which the star formed (Santos et al. 2004; Pinsonneault et al. 2001). In this scenario planet formation would be more prolific in a metal-rich environment (Ida & Lin 2004). Others suggest that the host stars were enriched by

[1]Based on data from the FLWO 1.2m telescope
[2]Hubble Fellow
[3]Also at Konkoly Observatory

the infall of other giant gas planets (Lin 1997) or small planetary bodies like asteroids (Murray & Chaboyer 2002).

The observed lack of planets in the core (Gilliland et al. 2000) and the uncrowded outer regions (Weldrake et al. 2005) of the low metallicity ([Fe/H]$= -0.7$) globular cluster 47 Tuc suggests that the source of the metallicity enhancement in planet hosts is most likely "primordial". Open clusters offer the possibility of observing a large number of stars with the same, known a priori metallicity. NGC 6791, with its high metallicity and large number of stars, seems particularly well suited as a target for transiting planet search.

Targeting open clusters also eliminates the problem of false detections due to blended eclipsing binary stars, which are a significant contaminant in the Galactic field searches (over 90% of all candidates; Konacki et al. 2003; Udalski et al. 2002a, 2002b). Blending causes a large decrease of the depth of the eclipses and mimics the transit of a much smaller object, such as a planet. As opposed to dense star fields in the disk of our Galaxy, open clusters located away from the galactic plane are sparse enough for blending to be negligible.

There are two key elements in a survey for transiting planets. The most commonly emphasized requirement is the high photometric precision, at the 1% level. The more often overlooked factor is the need for very extensive temporal coverage.

Extensive temporal coverage is important because even for planets with periods between 1 and 2 days, the fractional transit length is only $\sim$5% of the period, and it drops to $\sim$2% for periods 2-10 days. During the remaining 95-98% of the period the system is photometrically indistinguishable from stars without transiting planets. To our best knowledge, PISCES is the most extensive search for transiting planets in open clusters in terms of temporal coverage with a 1 m telescope.

NGC 6791 has been previously searched for transiting planets by Bruntt et al. (2003), who found three transit-like events and seven other lower probability events which may possibly be due to instrumental effects. Of the three best candidates, none exhibited more than one transit and only one is located on the cluster main sequence. Bruntt et al. (2003) used the 2.5 m NOT telescope, which allowed them to obtain higher photometric precision and denser time sampling, but their temporal coverage was much inferior to ours: $\sim$24 hours spread over 7 nights, compared to our > 300 hours, collected over 84 nights.

The paper is arranged as follows: §2 describes the observations, §3 summarizes the reduction procedure, §4 outlines the search strategy for transiting planets, §5 gives an estimate of the expected number of transiting planet detections, §6 describes the candidates previously reported by Bruntt et al. (2003) and §7 contains the variable star catalog. Concluding remarks are found in §8.

2. Observations

The data analyzed in this paper were obtained at the Fred Lawrence Whipple Observatory (FLWO) 1.2 m telescope using the 4Shooter CCD mosaic with four thinned, back side illuminated AR coated Loral 2048^2 CCDs (Szentgyorgyi et al. in preparation). The camera, with a pixel scale of $0\farcs33$ pixel^{-1}, gives a field of view of $11\farcm4 \times 11\farcm4$ for each chip. The cluster was centered on Chip 3 (Fig. 1). The data were collected during 84 nights, from 2001 July 9 to 2003 July 10. A total of 1118×900 s R and 233×450 s V-band exposures were obtained. The V-band dataset was supplemented with 93×450 s exposures collected between 19 September 1998 and 5 November 1999 (previously analyzed by Mochejska, Stanek & Kaluzny 2003).

3. Data Reduction

3.1. *Image Subtraction Photometry*

The preliminary processing of the CCD frames was performed with the standard routines in the IRAF ccdproc package.[1]

Photometry was extracted using the ISIS image subtraction package (Alard & Lupton 1998; Alard 2000), as described in detail in Paper I.

The ISIS reduction procedure consists of the following steps: (1) transformation of all frames to a common (x, y) coordinate grid; (2) construction of a reference image from several of the best

[1]IRAF is distributed by the National Optical Astronomy Observatories, which are operated by the Association of Universities for Research in Astronomy, Inc., under cooperative agreement with the NSF.

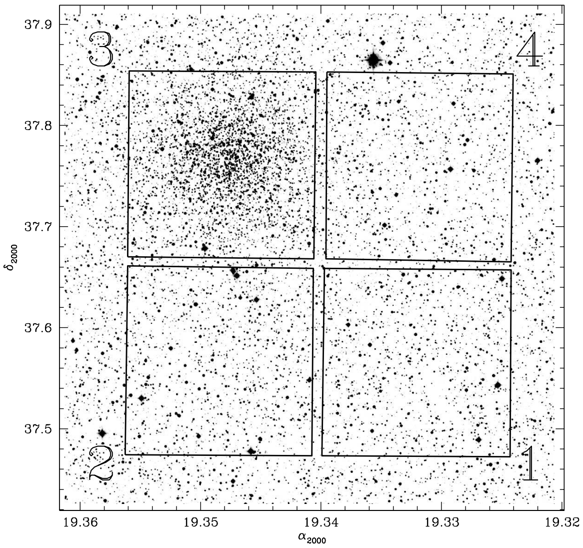

Fig. 1.— Digital Sky Survey image of NGC 6791 showing the field of view of the 4Shooter. The chips are numbered clockwise from 1 to 4 starting from the bottom left chip. NGC 6791 is centered on Chip 3. North is up and east is to the left.

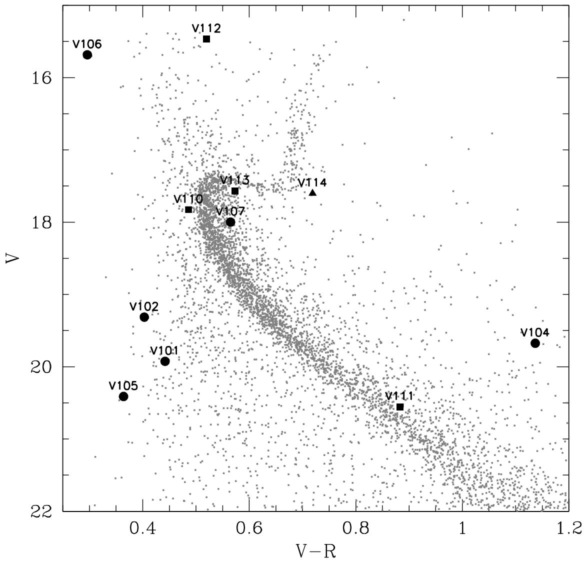

Fig. 2.— $V/V-R$ color-magnitude diagram for Chip 3, centered on NGC 6791. Newly discovered eclipsing binaries are plotted with circles, other periodic variables with squares and the non-periodic variable with a triangle.

exposures; (3) subtraction of each frame from the reference image; (4) selection of stars to be photometered and (5) extraction of profile photometry from the subtracted images.

All computations were performed with the frames internally subdivided into four sections (`sub_x=sub_y=2`). Differential brightness variations of the background were fit with a second degree polynomial (`deg_bg=2`). A convolution kernel varying quadratically with position was used (`deg_spatial=2`). The psf width (`psf_width`) was set to 33 pixels and the photometric radius (`radphot`) to 5 pixels. The reference images were constructed from 25 best exposures in R and 16 in V.

We slightly modified the reduction pipeline described in Paper I by introducing a procedure to remove photometry from epochs where a star was located in the proximity of bad columns. This task was somewhat complicated by the fact that the original `interp` program uses spline functions to remap each image to the template's (x, y) coordinate grid. If an image is masked before transformation, masked regions will spread over adjacent columns in the remapped image. To avoid this problem, we performed a linear transformation of the bad pixel masks for each image using the coefficients output by the `fitn` program. The shifted masks were applied to subtracted images. The `Cphot` program was modified, so that it ignored epochs where a bad pixel was within `radphot` pixels of a star's centroid.

3.2. *Calibration*

The transformations of instrumental magnitudes to the standard system were derived from observations of 15, 17, 15 and 17 stars on Chips 1-4, respectively, in four Landolt (1992) standard fields, collected on 2002 May 18. Transformations in the following form were adopted:

$$v = V + a_1 + a_2(V - R) + a_3(X - 1.25)$$
$$v - r = b_1 + b_2(V - R) + b_3(X - 1.25)$$
$$r = R + c_1 + c_2(V - R) + c_3(X - 1.25)$$

where X is the airmass. Table 1 lists the coefficients a_i, b_i, c_i and the rms scatter between the observed and calculated standard VR magnitudes.

These coefficients were used to calibrate the photometry from the images of the cluster taken

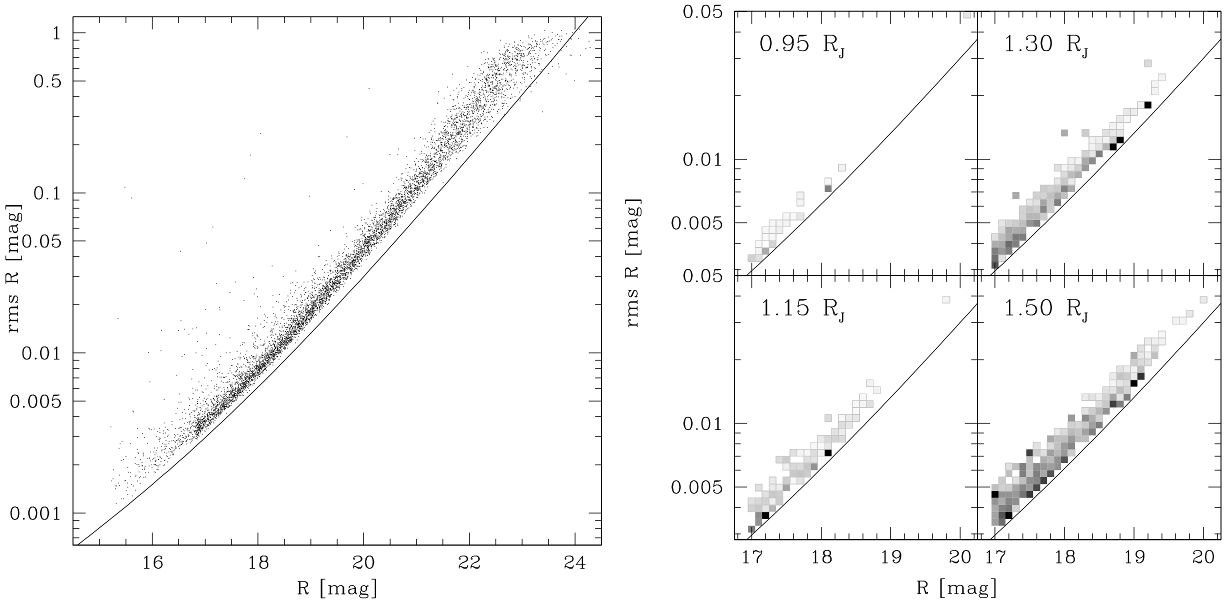

Fig. 3.— Left panel: The rms scatter of the R-band light curves for stars on Chip 3 with at least 650 data points. The continuous curve indicates the photometric precision limit due to Poisson noise of the star and average sky brightness. Right panel: The detection efficiency of 0.95, 1.15, 1.30 and 1.50 R_J planets as a function of magnitude and rms scatter (white: 0%, black 100%), determined in §5.3.

during the same night as the standards. The magnitudes from the reference images were transformed using the same color and extinction coefficients. The offsets were determined relative to the calibrated photometry from cluster images taken on the standard night. Figure 2 shows the calibrated V/V-R color-magnitude diagram (CMD) for the Chip 3 reference image[2].

A comparison of our V-band magnitudes with the photometry of Stetson, Bruntt & Grundahl (2003) reveals offsets of 0.048, 0.027, 0.047 and 0.009 mag in Chips 1-4, based on 20, 303, 3423 and 280 stars above $V = 20$, respectively. We also find an offset of 0.022 mag in V between our Chip 3 and Mochejska et al. (2003) data.

The VR light curves were converted from differential flux to instrumental magnitudes using the method described in Paper I. Instead of Eq. (1) from Paper I, we used the following relation to compute the total flux corresponding to the i-th image, c_i:

$$c_i = c_{ref} - \Delta c_i \tag{1}$$

where $\Delta c_i = c_{ref} - c_i$ is the flux on the i-th subtracted image and c_{ref} is the total flux on the reference image. This method should yield more accurate results because it is based on the reference image which has a higher S/N ratio than the template image used previously. The instrumental magnitudes were transformed to the standard system by adding offsets, computed individually for each star, between the instrumental and calibrated reference image magnitudes.

3.3. *Astrometry*

Equatorial coordinates were determined for the R-band reference image star lists. The transformation from rectangular to equatorial coordinates was derived using 964, 1012, 1476 and 951 transformation stars from the USNO B-1 catalog (Monet et al. 2003) in Chips 1 through 4, respectively. The mean of the absolute value of the deviation between the catalog and the computed coordinates for the transformation stars was $0\farcs13$ in right ascension and $0\farcs11$ in declination.

[2]The calibrated VR photometry is available from the authors via the anonymous ftp on cfa-ftp.harvard.edu, in the /pub/bmochejs/PISCES directory.

4. Search for Transiting Planets

4.1. *Further Data Processing*

We rejected 157 R-band epochs where less than 5000 stars were detected on Chip 3 by DAOphot (Stetson 1987), and 25 other bad quality images from three nights. This left us with 936 highest quality R-band exposures with a median seeing of $2''.1$. We also removed 8 V-band images, which left us with 318 exposures with a median seeing of $2''.3$.

In the light curves we noticed the presence of offsets between different runs. This may be due to the periodic UV flooding of the CCD camera, which alters its quantum efficiency as a function of wavelength. To prevent the transit detection algorithm from mistaking these changes in brightness for transits, we added offsets between the runs, individually for each light curve, so that the median magnitude was the same during each run. There were nine runs, each spanning from 44 to 187 data points. Typical sizes of the offsets were 0.008 mag for stars below $R = 18$ and 0.018 mag for stars between $R = 18$ and 19. As described in §5.6, this procedure greatly improves our detection efficiency.

The left panel of Fig. 3 shows the rms scatter of the R-band light curves for stars on Chip 3 with at least 650 data points. The continuous curve indicates the photometric precision limit due to Poisson noise of the star and average sky brightness. The right panel shows the detection efficiency of 0.95, 1.15, 1.30 and 1.50 R_J planets as a function of magnitude and rms scatter (white: 0%, black 100%), determined in §5.3.

4.2. *Selection of Transiting Planet Candidates*

For further analysis we selected stars with at least 650 out of 936 good epochs and light curve rms below 0.05 mag. Stars above the main sequence turnoff ($R = 17$) were rejected due to their large radii and, hence, very small expected transit depths (below 0.4%). This left us with 3074 stars on Chip 3, and 2975 on Chips 1, 2 and 4 (825, 1091 and 1059 stars, respectively).

To select transiting planet candidates we used the box-fitting least-squares (BLS) method (Kovács, Zucker, & Mazeh 2002). Adopting a cutoff of 6 in Signal Detection Efficiency (SDE) and 9 in effective signal-to-noise ratio (α), we selected

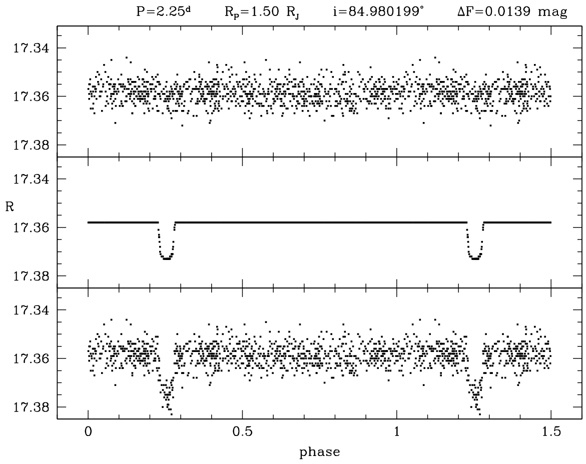

Fig. 4.— The original, model and combined light curves (upper, middle and lower panels, respectively) for a star with $R = 18.01$ and a planet with a period of 3.25 days, radius of 1.3 R_J and inclination of 88°.

185 candidates on Chip 3 and 39 on Chips 1, 2 and 4 (12, 16 and 11 candidates, respectively). We found three candidates on Chip 3, which were rejected as false detections upon closer examination. They had similar coordinates on the image and their periods were all nearly exact integral multiples of 0.9244 days. We have found 13 other stars within a distance of 50 pixels whose periods were also such multiples. An examination of the period distribution of all stars revealed significant peaks at 4, 6 and 8 times 0.9244 days. We did not find any other good transiting planet candidates.

5. Estimate of the Number of Expected Detections

The number of transiting planets we should expect to find, N_P, can be derived from the following equation:

$$N_P = N_* f_P D \tag{2}$$

where N_* is the number of stars with sufficient photometric precision, f_P is the frequency of planets within the investigated period range and D is the detection efficiency, which accounts for random inclinations. In §§5.1, 5.2 and 5.3 we determine f_P, N_* and D.

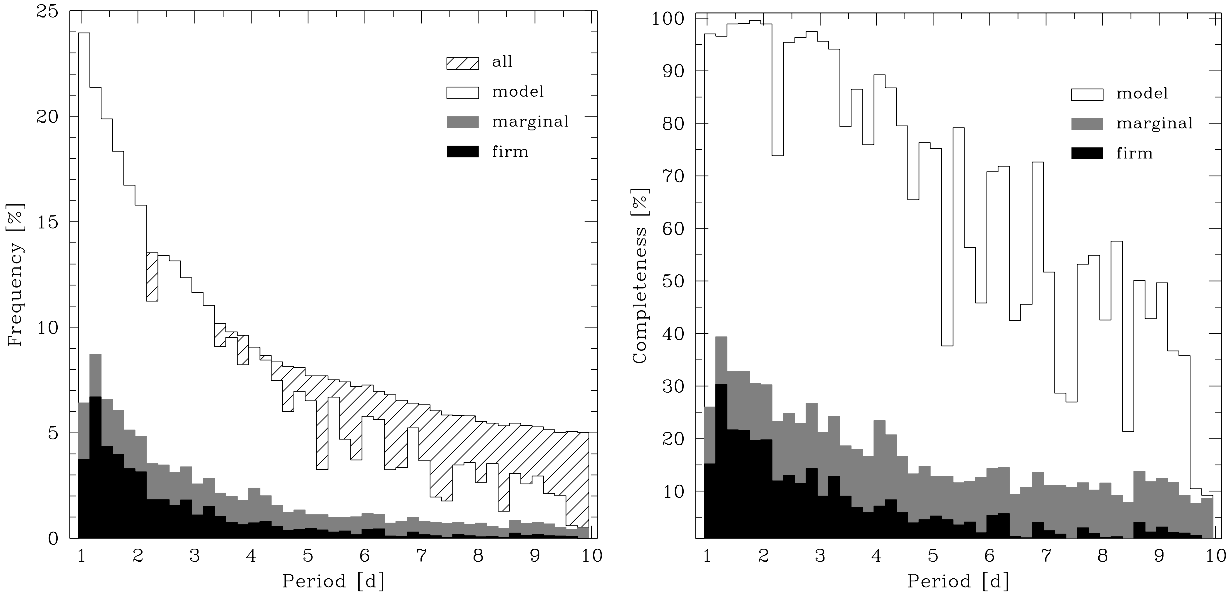

Fig. 5.— Detection efficiency of transiting planets as a function of their period, relative to planets with all inclinations (left panel) and all transiting planets (right). Shown are the distributions for all transiting planets (hashed histogram), detections in the model light curves (open) and marginal (gray) and firm (solid) detections in the combined light curves.

5.1. *Planet Frequency*

The frequency of planets is known to increase with the host star's metallicity. From Figure 7 in Santos et al. (2004), the frequency of planets for stars with [Fe/H] = +0.3 − +0.4 dex is ∼28%, and it drops to ∼2.5% for metallicities below [Fe/H] = +0.1 dex.

The percentage of planets with periods below 10 days is 14.6% in the Santos et al. (2004) sample. As of 16 November 2004, the corresponding fractions for the planet lists on exoplanets.org[3] and The Extrasolar Planets Encyclopaedia[4] were 15.3% and 15.8% (excluding planets detected via transits). In further analysis, we adopt the value of 15% as the fraction of planets with periods below 10 days.

Combining these two numbers yields f_P=4.2% for the high metallicity cluster stars and 0.375% for field stars. Please note that the latter estimate is considerably lower than the commonly adopted frequency of 1%.

[3]http://exoplanets.org/planet_table.txt

[4]http://www.obspm.fr/encycl/cat1.html

5.2. *The Number of Cluster and Field Stars*

Most of the cluster is contained on Chip 3 but its main sequence (MS) is also discernible on Chips 1, 2 and 4. To obtain a rough estimate of the number of stars belonging to the cluster, we determined the MS fiducial line and counted as members all stars within 0.06 mag of it in $V-R$, on all four chips. This gives 246, 381, 2201 and 350 "cluster" stars and 577, 710, 852 and 706 "field" stars on Chips 1-4, respectively. Twenty six stars did not have V-band data, and we assumed that they belong to the field. There are a total of 3178 "cluster" and 2871 "field" stars. There are more "field" stars on Chip 3 than on the other chips, which means that some of them belong to the cluster and our color cutoff is not too liberal. On the other hand, a small fraction of the "cluster" stars are field stars, so these two biases should cancel out to some extent.

5.3. *Detection Efficiency*

In order to characterize our detection efficiency, we inserted model transits into the observed light curves, and tried to recover them using the BLS

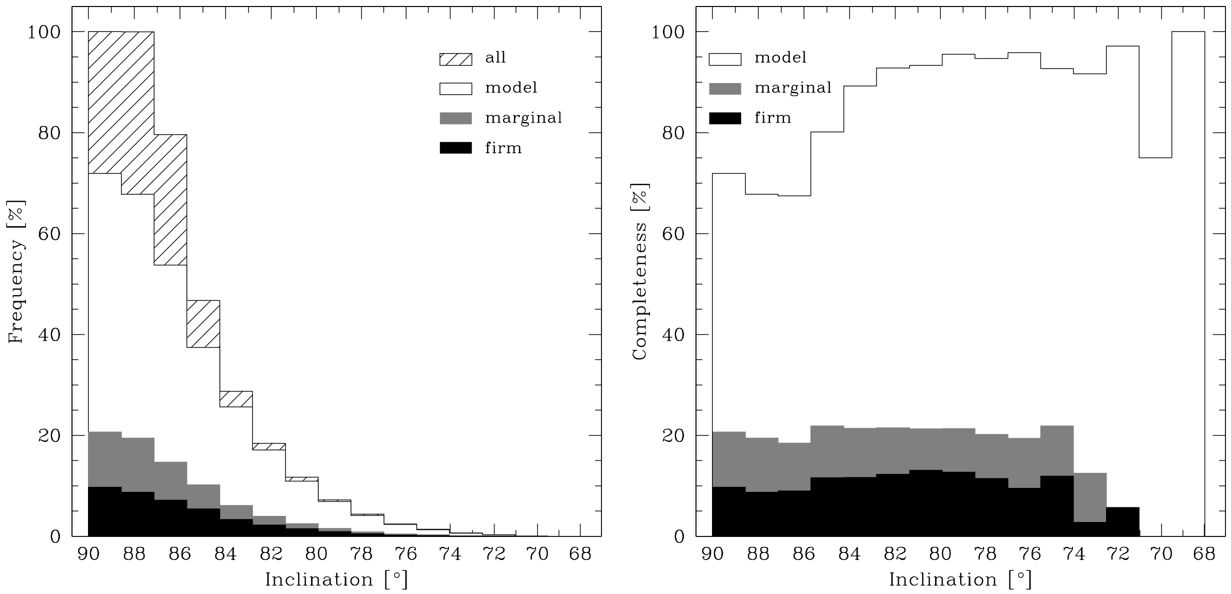

Fig. 6.— Detection efficiency of planetary transits as a function of their inclination, relative to planets with all inclinations (left panel) and all transiting planets (right).

method.

5.3.1. *Model Transit Light Curves*

The model transit light curves were defined by five parameters: the transit depth, ΔF, total transit duration, t_T, transit duration between ingress and egress, t_F (the "flat" part of the transit), the period of the planet, P and the limb darkening coefficient, u.

The first three parameters were computed from equations (1), (15) and (16) in Seager & Mallén-Ornelas (2003):

$$\Delta F = \left(\frac{R_p}{R_*}\right)^2 \tag{3}$$

$$\left(\frac{t_F}{t_T}\right)^2 = \frac{\left(1-\frac{R_p}{R_*}\right)^2 - \left(\frac{a}{R_*}\cos i\right)^2}{\left(1+\frac{R_p}{R_*}\right)^2 - \left(\frac{a}{R_*}\cos i\right)^2} \tag{4}$$

$$t_T = \frac{PR_*}{\pi a}\sqrt{\left(1+\frac{R_P}{R_*}\right)^2 - \left(\frac{a}{R_*}\cos i\right)^2} \tag{5}$$

Equations (4) and (5) are valid for $t_T \pi P \ll 1$. The radius of the planetary orbit, a, can be derived from the star's mass, M_*, and Kepler's third law, with the planet's mass $M_p \ll M_*$:

$$a = \left[\frac{P^2 G M_*}{4\pi^2}\right]^{1/3} \tag{6}$$

The radius and mass of the star, R_* and M_*, were interpolated, as a function of absolute R-band magnitude, M_R, from the highest metallicity (Z = 0.03) 7.943 Gyr isochrone of Girardi et al. (2000). A distance modulus $(m - M)_R = 13.36$ mag was used to bring the observed R-band magnitudes to the absolute magnitude scale (Chaboyer et al. 1999).

The effects of limb darkening were simulated using the linear approximation first introduced by Milne (1921):

$$I(\mu) = (1 - u(1-\mu)) \tag{7}$$

where u is the limb darkening coefficient, $\mu = cos(\theta)$, θ is the angle between the line of sight and the emergent flux, and $I(1)$ is the intensity at the center of the disk. We used the grid of R-band limb darkening coefficients, given as a function of gravity, G, and temperature, T_{eff}, by Claret, Diaz-Cordoves & Gimenez (1995). For each star, its G and T_{eff} were determined from Girardi et al. (2000) isochrones and u was interpolated from four closest points in G and T_{eff} in the Claret et

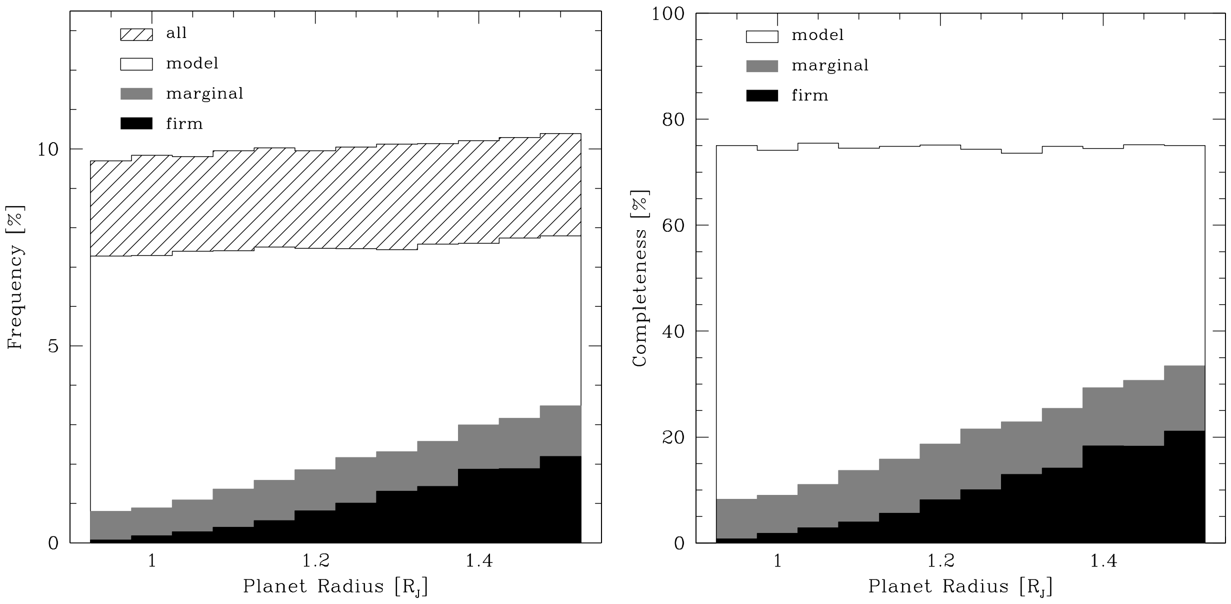

Fig. 7.— Detection efficiency of planetary transits as a function of their radius, relative to planets with all inclinations (left panel) and all transiting planets (right).

al. (1995) grid.

In addition to P, the equations contain two other free parameters: the planet radius, R_P and the inclination of the orbit, i. A fourth parameter which affects the detectability of a planet is the epoch of the transits, T_0.

5.4. *Test Procedure*

We investigated the range of parameters specified in Table 2, where P is expressed in days, R_P in Jupiter radii (R_J), T_0 as a fraction of period. We examined the range of periods from 1.05 to 9.85 days and planet radii from 0.95 to 1.5 R_J, with a resolution of 0.2 days and 0.05 R_J, respectively. For T_0 we used an increment of 5% of the period, and a 0.025 increment in $\cos i$. The total number of combinations is 432000.

For each combination of parameters, a random star was chosen without replacement from the sample of 3074 stars on Chip 3. When the sample was exhausted, it was reset to the original list. The "observables" ΔF, t_T and t_F were computed and when $t_T \geq 0.5^h$ two light curves were generated: the **model** transit light curve, and the observed light curve combined with the model (hereafter referred to as the **combined** light curve). Figure 4 shows the original, model and combined light curves (upper, middle and lower panels, respectively) for a star with $R = 17.36$ and a planet with a period of 2.25 days, radius of 1.5 R_J and inclination of 85°. The amplitude of the transit is 0.0139 mag, and the mass and radius of the star, taken from the models, are 1.03 $M_\odot$ and 1.28 $R_\odot$.

To assess the impact of the procedure to correct for offsets between the runs on our detection efficiency, we investigated three cases, where the correction was applied:

A. after inserting transits,

B. before inserting transits,

C. was not applied at all.

Case (B) will give us the detection efficiency if our data did not need to be corrected, and case (C) if we did not apply the corrections. Case (A) will give us our actual detection efficiency, and its comparison with cases (B) and (C) will show how it is affected by the applied correction procedure.

This required us to run two sets of simulations: on the original (cases A and C) and corrected (case B) light curves. In both simulations the same list of parameter and star combinations was used.

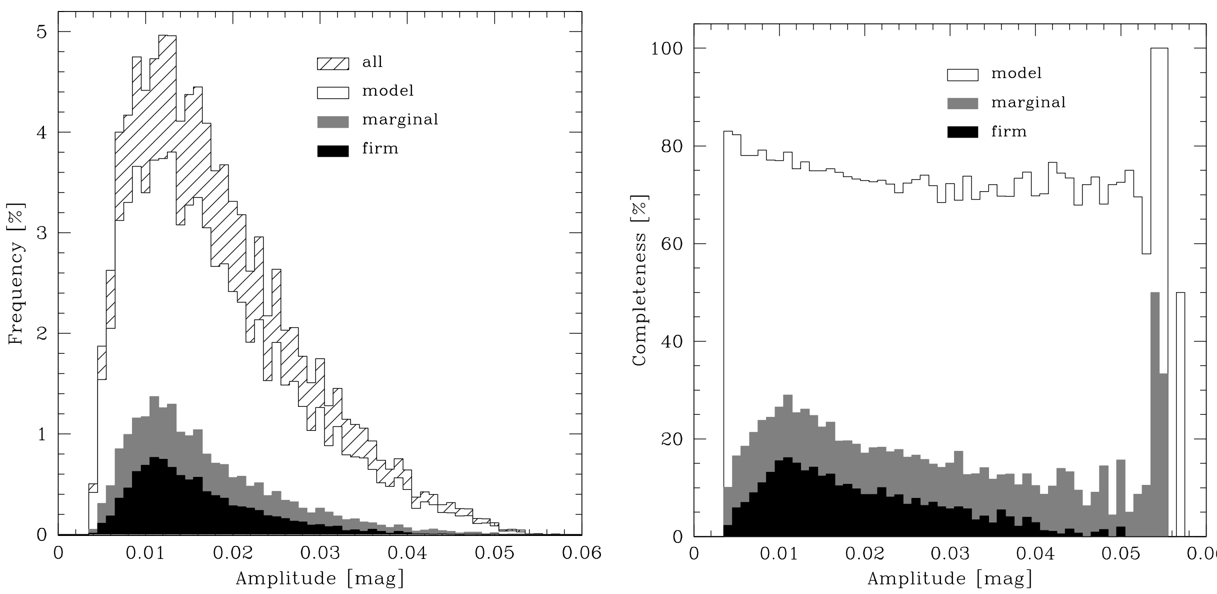

Fig. 8.— Detection efficiency of planetary transits as a function of their amplitude, relative to planets with all inclinations (left panel) and all transiting planets (right).

5.5. *Detection Criteria*

An examination of the frequency of recovered periods, relative to the input period, revealed that only the peaks at 1, 2 and $\frac{1}{2}$ P_{inp} are distinct. Other aliases blend in with the background of the incorrectly recovered periods, so we have disregarded them.

A transit was flagged as detected if:

1. The period recovered by BLS was within 2% of the input period P_{inp}, 2 P_{inp} or $\frac{1}{2}$ P_{inp},
2. The BLS statistics were above the following thresholds: $SDE > 6$, $\alpha > 9$.

These detections will be referred to hereafter as *firm*. Detections where only condition (1) was fulfilled will be called *marginal*.

5.6. *Detection Efficiency*

The results of the tests are summarized in Table 3, which lists the test type (A-C), the number and percentage of transits with $t_T \geq 0.5^h$ (out of the 432000 possible parameter combinations), and the numbers and percentages (relative to the total number of transits in column 2) of transits detected in the model light curves, and of marginal and firm detections in the combined light curves.

Figures 5-8 show the dependence of the detection efficiency on period, inclination, planet radius and transit amplitude. The hashed, open, gray and solid histograms denote distributions for all transiting planets, planets detected in the model light curves, and marginal and firm detections in the combined light curves, respectively. Left panels show the frequency of transits and transit detections relative to planets with all inclinations. Right panels show the detection completeness normalized to all transiting planets (plotted as hashed histograms in left panels).

The tests show that 10% of planets with periods 1-10 days will transit their parent stars. This frequency drops from ~24% at $P = 1^d$ to ~5% at $P = 10^d$. All planets with inclinations $87 - 90°$ transit their host stars, and this fraction drops to ~80% for $i = 86°$ and ~5% for $i = 78°$. The frequency of transits increases very weakly with planet radius. The distribution of transit amplitudes has a wide peak stretching from 0.6% to 2%, centered on ~1.3%.

The percentage of detections for the model light curves illustrates the limitation imposed on our detection efficiency by the temporal coverage alone. Due to incomplete time sampling, we are restricted to 75% of all planets with periods between 1 and 10 days. For periods below 4 days, our temporal coverage is sufficient to detect $\sim$90% of all transiting planets, and drops to $\sim$50% at $P = 9$ days. The detection completeness increases with decreasing inclination because at lower i only short period planets can transit their host stars. It does not depend on the planet radius, and it decreases with increasing transit amplitude.

The source of the dependence of the detection completeness on transit amplitude is not as straightforward as for the other correlations. The amplitude depends on the radii of the star and planet. Since the detection completeness was found to be largely independent of the planet radius, the observed trend must stem from its dependence on the host star's radius, which is a function of its magnitude. Such a correlation is indeed observed, with completeness increasing for brighter stars (not shown here). The link between the temporal coverage and magnitude comes from the observed increase in the number of points in the light curve with decreasing magnitude.

For cases A, B and C, we *marginally* detect 20%, 21% and 13% of all transiting planets, and *firmly* detect 10%, 11% and 4.6%, respectively. Transiting planets with firm detections constitute 83%, 84% and 64% of all stars with $SDE > 6$ and $\alpha > 9$. Adding offsets between runs (case A) decreases the number of firm detections by 7%, compared to the desired case, where no offsets would be required (case B). If the offsets were not corrected (case C), we would detect only 46% of the transiting planets detected in case A.

The detection completeness for firm detections peaks at 20% for periods $1-2^d$ and decreases with period more steeply than model detections. It does not show a marked dependence on inclination, and strongly increases with increasing planet radius, from below 2% at 1 R_J to over 20% at 1.5 R_J. This is also apparent in the right panel of Fig. 3, which shows the detection efficiency of 0.95, 1.15, 1.30 and 1.50 R_J planets as a function of magnitude and rms scatter (white: 0%, black 100%).

The detection efficiency peaks at an amplitude of $\sim$1%, due to the most favorable ratio between the transit amplitude and photometric accuracy for this amplitude/magnitude range.

The efficiency of *firm* transiting planet detections, relative to planets with all orbital inclinations, D, is $4323/432000 = 1.0\%$.

5.7. *Number of Transiting Planets Expected*

In §§ 5.1-5.3 we determined the planet frequency f_P to be 4.2% for cluster stars and 0.375% for field stars, the number of stars in the cluster and field as 3178 and 2871 and our detection efficiency D to be 1.0%. We should thus expect 1.34 transiting planets in the cluster and an additional 0.11 of a planet among field stars.

5.8. *Discussion*

Figure 5 demonstrates that our temporal coverage is not the limiting factor. To increase the number of expected planets it would be necessary to improve the photometric precision. The weather and seeing conditions turned out to be inferior to what we were expecting. A better quality CCD and a telescope with a larger diameter and/or better observing conditions would be required to improve the chances for a successful transiting planet search in NGC 6791.

The estimate of 1.45 expected transiting planets is not high enough to enable us to draw any conclusions from the fact that we have not detected any such events.

The precision of this estimate is largely limited by the uncertainty in one of our basic assumptions – the distribution of planetary radii. This distribution is not precisely known, and changing it will have a marked effect on the final result. Adopting a distribution of planetary radii from 1.0 to 1.35 R_J, corresponding to the radius range spanned by the six known transiting planets (Konacki et al. 2004) would lower D from 1.0% to 0.7%. This translates to 1.08 detections, compared to 1.45 with the original radius distribution – a 26% decrease.

In Paper I we made the assumption that the planetary radii would span the range 1-3 R_J, based on the radius of 1.347 R_J for the only known transiting planet at the time, HD 209458b (Brown et al. 2001). A simulation for planets in the radius range 1.5-3.0 R_J shows that 11% of them transit their parent stars, 75% are detected in the model light curves, and 56% and 45% are marginal and firm detections in the combined light curves. Assuming that planet radii are distributed evenly

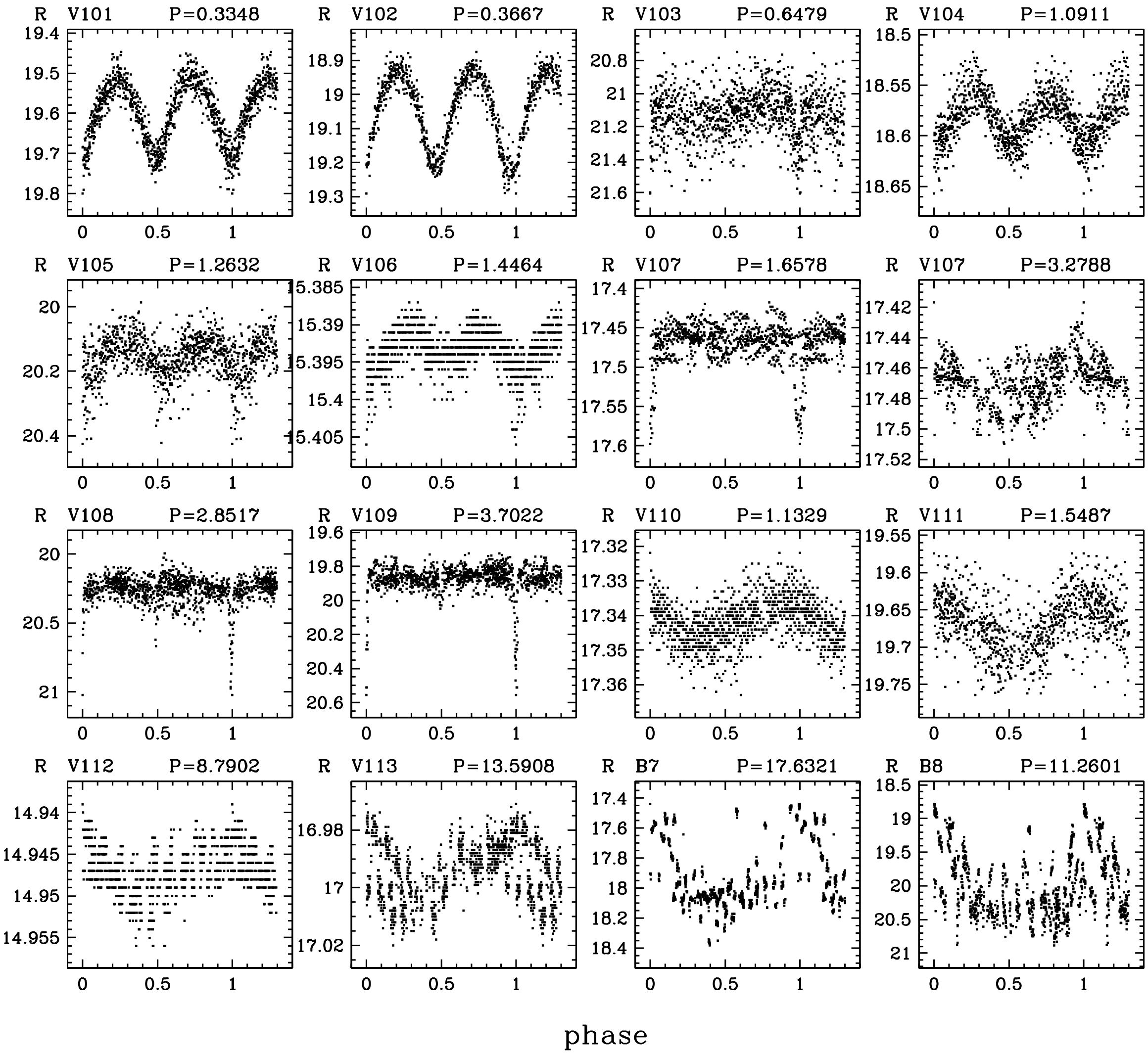

Fig. 9.— The R-band light curves of nine new eclipsing binaries, four new other periodic variables, and cataclysmic variables B7 and B8. V107 is phased with two detected periods.

between 1 and 3 R_J would give the percentage of firm detections of 37% and detection efficiency $D = 4.0\%$, which translates into 5.33 expected detections in the cluster and 0.43 in the field. Our lack of detections does not favor such large planetary radii, in agreement with observations (Fig. 5 in Konacki et al. 2004) and current models (Bodenheimer, Laughlin & Lin 2003; Burrows et al. 2004; Chabrier et al. 2004, Kornet et al. 2005).

6. Previously Reported Candidates

We examined the light curves of the transiting planet candidates reported by Bruntt et al. (2003). None of them were found to exhibit convincing periodic transits or eclipses. Even with our lower photometric accuracy, in most cases we should have detected a periodicity, if we had observed several transits. The rms of our R-band light curves is 0.009 for T10 and $0.003 - 0.006$ for the remaining candidates.

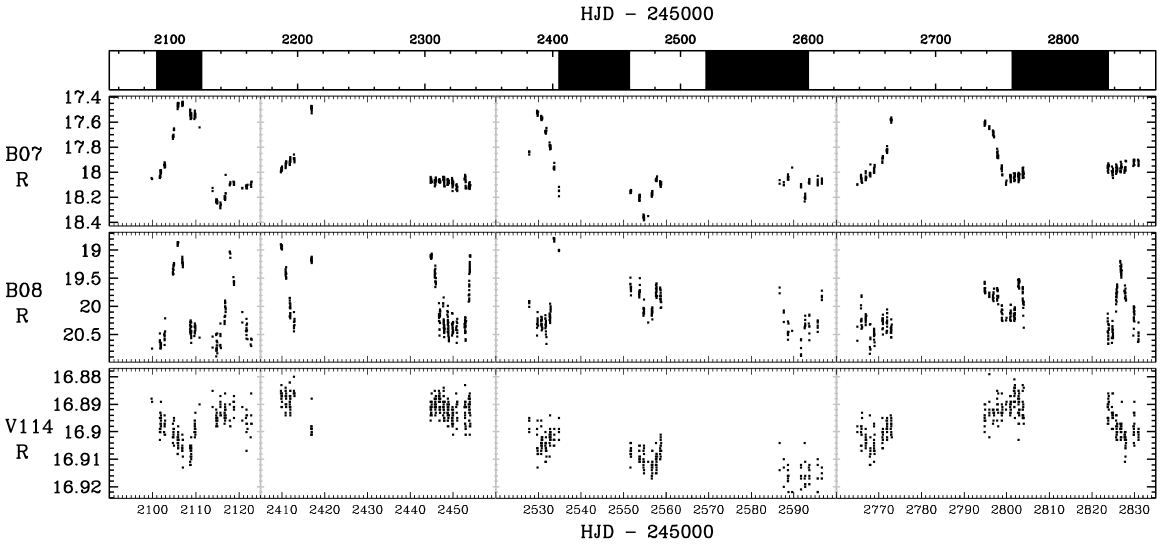

Fig. 10.— The R-band light curves of the cataclysmic variables B7 and B8 and the new variable V114. The top window illustrates the distribution in time of the four sub-windows plotted for the variables.

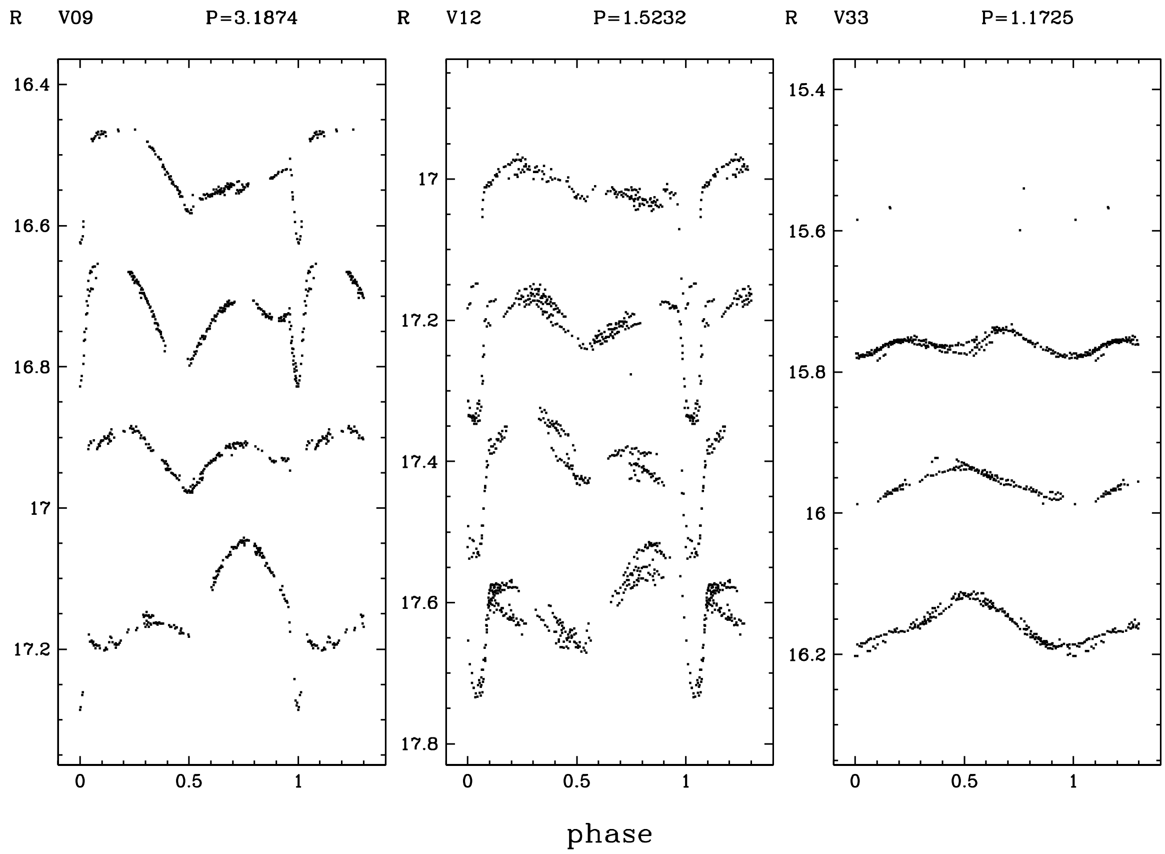

Fig. 11.— The R-band light curves of the eclipsing binaries V9, V12 and V33.

7. Variable Stars

We also extracted the light curves of known variable stars and searched for new ones by running BLS in the period range 0.1-10 days. In Tables 4-6 we list their revised parameters. We note, for the record, that variables V85, V88 and V96, reported as new discoveries by Bruntt et al. (2003), are the same as V76, V77 and V56 reported earlier by Kaluzny (2003) and in Paper I. We have reclassified V40 and V41 as eclipsing binaries.

We have discovered 14 new variables: 1, 4, 7 and 2 on Chips 1-4, respectively. Their parameters are listed in Tables 4 and 6 and their light curves are shown in Figures 9 and 10.[5] They are also plotted on the CMD in Fig. 2. Variables V101-V109 are eclipsing binaries: V101, V102, V104-V106 are W UMa type contact systems, V103, V107-V109 are detached or semi-detached binaries. In addition to eclipses, V107 displays out of eclipse variability with a period almost exactly twice as long as the orbital period. In Fig. 9 it is shown phased with both periods. For clarity, points in the eclipse have been removed from the light curve phased with the longer period. The other periodic variables, V110-V113, are most likely spotted stars. The shape of the light curve of V113 varies noticeably with time.

The non-periodic variable V114 is located slightly redward of the base of the red giant branch. If it belongs to the cluster, it might be a member of the recently proposed class of variable stars termed "red stragglers" (Albrow et al. 2001) or "sub-subgiant stars" (Mathieu et al. 2003). Thus far, the origin and evolutionary status of these stars remains unknown.

In Fig. 10 we show the light curves of the cataclysmic variables B7 and B8. In Fig. 9 they are phased with cycle lengths 17.6 and 11.3 days, respectively. Equally good fits to the B7 and B8 data are given by periods of 22.12 and 17.75 days, closer to the cycle lengths of 25.41 and 17.73, reported by Mochejska, Stanek & Kaluzny (2003). More observations are required to firmly establish the cycle lengths of these variables.

In Fig. 11 we show the light curves of three RS CVn type binaries V9, V12 and V33, plotted separately for four time intervals: 2001 July 9 - August 1, 2002 May 14 - June 28, 2002 September 10 - November 18 and 2003 May 5 - July 10. The shape of their light curves varies with time, especially for V12 and V33.

8. Conclusions

In this paper we have performed an extensive search for transiting planets in the very old, populous, metal rich cluster NGC 6791. The cluster was monitored for over 300 hours during 84 nights. We have not detected any promising transiting planet candidates. Assuming a planet frequency from radial velocity surveys, we estimate that we should have detected 1.5 transiting planets with periods between 1 and 10 days, with our photometric precision and temporal coverage. The main limitation on our detection efficiency was imposed by the photometric precision.

We have discovered 14 new variable stars in NGC 6791: nine eclipsing binaries, four other periodic variables and one non-periodic variable, bringing the total number of variables in this cluster to 111. We have also presented high photometric precision light curves, spanning two years, for all previously known variables. Many of them show changes in light curve shape, i.e. V9, V12 and V33 (Fig. 11). This phenomenon is most likely due to the evolution of magnetic spots on the surface of these stars.

Transiting planets have proven to be more challenging to detect than initially expected, as shown by the paucity of detections from the many searches under way in open clusters (i.e. Bruntt et al. 2003; UStAPS: Street et al. 2003; EXPLORE/OC: von Braun et al. 2004; STEPSS: Burke et al. 2004) and in the Galactic field (i.e. EXPLORE: Mallén-Ornelas et al. 2003; OGLE: Udalski et al. 2002a; STARE: Alonso et al. 2003; HAT: Bakos et al. 2004[6]). To date, only six planets have been discovered independently by transit searches, all of them in the field, and five of those were initially identified by OGLE (Udalski et al. 2002a, 2002b, 2002c, 2003; Alonso et al.

[5] The VR band photometry and finding charts for all variables are available from the authors via the anonymous ftp on cfa-ftp.harvard.edu, in the /pub/bmochejs/PISCES directory.

[6] For a more complete list of transiting planet searches, please refer to `http://star-www.st-and.ac.uk/~kdh1/transits/table.html` and `http://www.obspm.fr/encycl/searches.html`

2004).

We would like to thank the FLWO 1.2 m TAC for the generous amount of time we were allocated to this project, the anonymous referee for a prompt and useful report, Scott Gaudi and Janusz Kaluzny for helpful discussions, Alceste Bonanos for her help in obtaining some of the data, Andrzej Kruszewski for granting us access to his light curve correction code and Peter McCullough for advice on rejecting bad epochs.

This research has made use of the USNOFS Image and Catalogue Archive operated by the United States Naval Observatory, Flagstaff Station (http://www.nofs.navy.mil/data/fchpix/), the Digital Sky Survey, produced at the Space Telescope Science Institute under U.S. Government grant NAG W-2166, the SIMBAD database, operated at CDS, Strasbourg, France and the WEBDA open cluster database maintained by J. C. Mermilliod (http://obswww.unige.ch/webda/).

Support for BJM, GAB and JNW was provided by NASA through Hubble Fellowship grants HST-HF-01155.02-A, HF-01170.01-A, HST-HF-01180.01-A from the Space Telescope Science Institute, which is operated by the Association of Universities for Research in Astronomy, Incorporated, under NASA contract NAS5-26555. KZS acknowledges support from the William F. Milton Fund.

REFERENCES

Alard, C. 2000, A&AS, 144, 363

Alard, C., Lupton, R. 1998, ApJ, 503, 325

Albrow, M. D., Gilliland, R. L., Brown, T. M., Edmonds, P. D., Guhathakurta, P., & Sarajedini, A. 2001, ApJ, 559, 1060

Alonso, R., et al. 2004, ApJ, 613, L153

Alonso, R., Belmonte, J. A., & Brown, T. 2003, Ap&SS, 284, 13

Bakos, G., Noyes, R. W., Kovács, G., Stanek, K. Z., Sasselov, D. D., & Domsa, I. 2004, PASP, 116, 266

Bodenheimer, P., Laughlin, G., & Lin, D. N. C. 2003, ApJ, 592, 555

Brown, T. M., Charbonneau, D., Gilliland, R. L., Noyes, R. W., & Burrows, A. 2001, ApJ, 552, 699

Bruntt, H., Grundahl, F., Tingley, B., Frandsen, S., Stetson, P. B., & Thomsen, B. 2003, A&A, 410, 323

Burke, C. J., Gaudi, B. S., DePoy, D. L., Pogge, R. W., & Pinsonneault, M. H. 2004, AJ, 127, 2382

Burrows, A., Hubeny, I., Hubbard, W. B., Sudarsky, D., & Fortney, J. J. 2004, ApJ, 610, L53

Chaboyer, B., Green, E. M., & Liebert, J. 1999, AJ, 117, 1360

Chabrier, G., Barman, T., Baraffe, I., Allard, F., & Hauschildt, P. H. 2004, ApJ, 603, L53

Claret, A., Diaz-Cordoves, J., & Gimenez, A. 1995, A&AS, 114, 247

Gilliland, R. L., et al. 2000, ApJ, 545, L47

Girardi, L., Bressan, A., Bertelli, G., & Chiosi, C. 2000, A&AS, 141, 371

Ida, S., & Lin, D. N. C. 2004, ApJ, 616, 567

Kaluzny, J. 2003, Acta Astronomica, 53, 51

Kaluzny, J., Udalski, A. 1992, Acta Astronomica, 42, 29

Konacki, M., Torres, G., Jha, S., & Sasselov, D. D. 2003, Nature, 421, 507

Konacki, M., Torres, G., Sasselov, D. D., & Jha, S. 2004, ApJ, submitted (astro-ph/0412400)

Kornet, K., Bodenheimer, P., Różyczka, M., & Stepinski, T. F. 2005, A&A, 430, 1133

Kovács, G., Zucker, S., & Mazeh, T. 2002, A&A, 391, 369

Landolt, A. U. 1992, AJ, 104, 340

Lin, D. N. C. 1997, ASP Conf. Ser., 121, 321

Mallén-Ornelas, G., Seager, S., Yee, H. K. C., Minniti, D., Gladders, M. D., Mallén-Fullerton, G. M., & Brown, T. M. 2003, ApJ, 582, 1123

Mathieu, R. D., van den Berg, M., Torres, G., Latham, D., Verbunt, F., & Stassun, K. 2003, AJ, 125, 246

Milne, E. A. 1921, MNRAS, 81, 361

Mochejska, B. J., Stanek, K. Z., & Kaluzny, J. 2003, AJ, 125, 3175

Mochejska, B. J., Stanek, K. Z., Sasselov, D. D., Szentgyorgyi, A. H., Westover, M., & Winn, J. N. 2004, AJ, 128, 312 (Paper II)

Table 1

Calibration Coefficients

	V				V-R				R			
chip	a_1	a_2	a_3	rms	b_1	b_2	b_3	rms	c_1	c_2	c_3	rms
1	2.8989	0.0585	0.1733	0.009	0.2089	1.0941	0.0305	0.016	2.6916	-0.0361	0.1338	0.014
2	3.2527	0.0627	0.1664	0.009	0.3349	1.1002	0.0178	0.010	2.9206	-0.0379	0.1370	0.011
3	2.7596	0.0734	0.1557	0.006	0.1937	1.0952	0.0430	0.006	2.5674	-0.0218	0.1056	0.008
4	2.8950	0.0548	0.1318	0.005	0.2623	1.0823	0.0011	0.015	2.6339	-0.0276	0.1239	0.013

Table 2

Parameter Range

Parameter	min	max	step	n_{steps}
P (days)	1.05	9.85	0.200	45
R_P (R_J)	0.95	1.50	0.050	12
T_0	0.00	0.95	0.050	20
$\cos i$	0.0125	0.9875	0.025	40

Table 3

Artificial transit test statistics

test	all transits		model		marginal		firm	
type	N	%	N	%	N	%	N	%
A	43371	10.0	32406	74.7	8737	20.1	4323	10.0
B	43367	10.0	32380	74.7	9173	21.2	4659	10.7
C	43371	10.0	32406	74.7	5754	13.3	1998	4.6

Table 4
Eclipsing binaries in NGC 6791

ID	α_{2000} [h]	δ_{2000} [∘]	P [d]	R_{max}	V_{max}	A_R	A_V
V22	19 20 18.7	37 30 29.8	0.2451	18.917	19.654	0.693	1.113
V01	19 20 47.6	37 44 32.0	0.2677	15.718	16.241	0.308	0.393
V23	19 20 19.0	37 47 16.0	0.2718	16.196	16.856	0.071	0.099
V02	19 21 17.5	37 46 00.2	0.2735	19.074	19.537	0.198	0.546
V24	19 19 58.5	37 35 44.0	0.2758	18.282	19.001	0.227	0.344
V25	19 19 42.3	37 42 48.1	0.2774	17.852	18.554	0.447	0.522
V06	19 21 02.7	37 48 48.9	0.2790	14.972	15.430	0.101	0.120
V26	19 20 44.9	37 33 42.6	0.2836	16.798	17.332	0.212	0.237
V05	19 20 46.5	37 48 47.8	0.3127	16.669	17.193	0.050	0.078
V03	19 21 15.8	37 46 09.7	0.3176	17.955	18.535	0.091	0.188
V04	19 20 54.2	37 48 23.8	0.3256	17.170	17.771	0.102	0.118
V27	19 20 10.7	37 38 56.5	0.3317	17.985	18.549	0.646	0.840
V101	19 21 05.6	37 38 25.3	0.3348	19.483	19.925	0.310	0.425
V102	19 19 31.0	37 32 16.0	0.3667	18.911	19.314	0.377	0.498
V28	19 19 43.8	37 35 30.2	0.3721	16.948	17.467	0.420	0.552
V40	19 19 39.0	37 37 01.0	0.3975	19.033	19.748	0.163	0.210
V29	19 21 17.3	37 45 05.2	0.4366	19.083	20.046	0.193	0.236
V41	19 20 51.0	37 48 24.7	0.4817	18.359	19.072	0.111	0.202
V103	19 20 35.6	37 35 45.0	0.6479	20.856	···	0.779	···
B04	19 21 12.9	37 45 51.3	0.7970	17.910	17.873	0.063	0.113
V11	19 20 33.3	37 48 16.6	0.8831	18.843	19.449	0.419	0.670
V104	19 20 43.3	37 34 40.6	1.0911	18.538	19.675	0.114	0.423
V33	19 20 39.8	37 43 54.4	1.1725	15.522	16.224	0.080	0.172
V30	19 19 43.0	37 30 06.9	1.1790	15.746	16.074	0.025	0.037
V80	19 21 06.5	37 47 27.8	1.2215	17.142	17.738	0.107	0.174
V105	19 20 39.1	37 33 36.2	1.2632	20.048	20.412	0.371	0.713
V106	19 21 10.7	37 45 31.6	1.4464	15.389	15.685	0.016	0.022
V43	19 20 39.6	37 38 30.7	1.5140	18.186	···	0.075	···
V12	19 20 42.9	37 50 56.5	1.5232	16.931	17.499	0.248	0.340
V107	19 21 18.2	37 45 41.8	1.6578	17.434	17.999	0.157	0.236
V32	19 20 27.6	37 47 14.2	2.0703	18.760	19.334	0.130	0.269
V34	19 20 09.2	37 44 10.7	2.4059	18.410	19.201	0.193	0.336
V36	19 19 56.4	37 34 12.6	2.6722	15.517	16.323	0.057	0.093
V108	19 21 09.4	37 49 24.5	2.8517	20.117	···	0.870	···
V09	19 20 47.9	37 46 37.4	3.1874	16.458	17.219	0.225	0.370
V37	19 21 18.2	37 51 07.0	3.2133	18.353	19.535	0.156	0.648
V35	19 20 44.1	37 30 42.8	3.2189	16.628	17.139	0.235	0.255
V31	19 21 02.5	37 47 09.3	3.3147	16.565	17.125	0.021	0.036
V109	19 20 33.8	37 47 37.4	3.7022	19.766	···	0.760	···
V38	19 21 03.7	37 46 05.9	3.8704	18.195	18.833	0.192	0.239
V60	19 21 00.7	37 45 45.0	7.4532	18.083	18.697	0.320	0.678
V20	19 20 54.3	37 45 34.7	7.4742	16.823	17.377	0.271	0.288
V39	19 21 00.5	37 38 22.8	7.6006	15.956	16.678	0.079	0.098
V14	19 20 51.7	37 45 24.8	10.9853	18.065	···	0.073	···
V18	19 20 49.4	37 46 09.2	17.6389	17.197	···	0.433	···
V61	19 19 42.9	37 29 07.4	19.3807	16.314	16.888	0.467	0.561

Table 5

Other periodic variables in NGC 6791

ID	α_{2000} [h]	δ_{2000} [$\circ$]	P [d]	$\langle R\rangle$	$\langle V\rangle$	A_R	A_V
V42	19 21 00.2	37 42 53.4	0.5064	18.954	19.597	0.035	0.044
V93	19 21 05.2	37 47 08.4	0.9941	16.473	16.925	0.003	0.004
V110	19 21 05.8	37 44 30.4	1.1329	17.342	17.828	0.005	0.006
V111	19 20 49.1	37 48 43.7	1.5487	19.672	20.555	0.033	0.030
V84	19 20 47.7	37 44 58.2	1.6258	18.989	19.836	0.021	0.027
V44	19 19 37.1	37 41 41.7	2.2544	17.782	18.410	0.013	0.019
V16	19 21 07.6	37 48 09.6	2.2664	17.276	17.850	0.019	0.024
V76	19 20 49.9	37 45 50.9	4.0924	17.585	18.270	0.030	0.034
V49	19 20 30.9	37 36 51.2	4.9923	15.266	15.802	0.007	0.007
V45	19 20 46.1	37 42 05.9	5.0883	16.463	17.083	0.007	0.010
V46	19 21 19.0	37 47 56.1	5.1287	17.930	18.688	0.033	0.037
V47	19 19 39.1	37 32 10.8	5.6066	18.737	19.978	0.024	0.011
V91	19 21 00.5	37 48 40.6	5.6411	17.611	18.097	0.004	0.004
V48	19 21 07.5	37 43 06.6	5.8019	17.003	17.558	0.018	0.013
V50	19 20 35.2	37 31 04.3	5.8812	16.055	16.544	0.011	0.008
V89	19 20 56.6	37 46 36.2	6.1577	18.226	19.078	0.025	0.053
V17	19 20 38.9	37 49 04.5	6.3656	17.279	17.949	0.020	0.020
V52	19 21 20.9	37 46 19.2	6.9933	17.016	$\cdots$	0.005	$\cdots$
V51	19 21 12.2	37 44 54.7	7.0315	19.257	19.971	0.032	0.025
V77	19 20 52.9	37 46 36.9	7.1810	16.206	16.744	0.003	0.004
V53	19 21 00.8	37 44 35.4	7.1822	18.257	18.803	0.011	0.006
V83	19 20 46.4	37 44 14.1	7.2915	18.683	19.392	0.013	0.017
V82	19 20 39.7	37 47 36.0	7.4983	18.522	19.064	0.018	0.008
V54	19 21 18.7	37 43 36.4	8.3141	15.929	16.524	0.010	0.010
V98	19 20 56.5	37 45 38.7	8.3405	16.418	$\cdots$	0.003	$\cdots$
V112	19 20 04.2	37 48 33.4	8.7902	14.947	15.467	0.003	0.002
V95	19 20 43.1	37 47 32.5	9.6832	18.509	19.147	0.014	0.010
V65	19 20 52.5	37 47 30.5	11.1091	15.645	16.272	0.004	0.006
V56	19 20 45.3	37 45 48.8	12.3832	16.518	17.081	0.006	0.003
V57	19 20 57.9	37 31 07.0	13.1536	17.460	18.359	0.010	0.007
V58	19 21 14.5	37 48 04.4	13.2597	17.028	17.544	0.015	0.016
V113	19 20 34.9	37 48 14.8	13.5908	16.995	17.568	0.009	0.013
V97	19 20 49.2	37 49 14.8	13.6206	15.813	16.517	0.003	0.004
V59	19 20 21.5	37 48 21.9	13.8331	17.221	17.781	0.056	0.049
V64	19 21 11.4	37 29 55.4	14.2427	15.882	16.473	0.005	0.012
V81	19 20 49.7	37 48 08.7	16.6182	16.373	16.905	0.003	0.005
V100	19 21 01.8	37 45 41.9	23.9468	16.544	17.151	0.024	0.021
V66	19 21 08.4	37 44 55.2	50.4976	15.372	16.119	0.068	0.074
V71	19 21 10.5	37 43 24.8	51.9430	16.563	17.291	0.057	0.067
V67	19 21 03.7	37 48 03.7	66.7944	16.180	16.959	0.056	0.071

Table 6
Miscellaneous variables in NGC 6791

ID	α_{2000} [h]	δ_{2000} [∘]	R_{max}	V_{max}	A_R	A_V
B07	19 21 07.4	37 47 56.5	17.448	17.581	0.819	0.919
B08	19 20 35.7	37 44 52.3	18.820	18.716	1.896	3.403
V10	19 21 11.8	37 47 58.1	18.922	19.642	0.103	0.435
V21	19 20 57.3	37 45 36.9	16.997	17.547	0.016	0.041
V62	19 21 03.0	37 43 51.8	18.618	19.189	0.105	0.214
V63	19 19 40.0	37 29 45.1	16.317	17.058	0.024	0.066
V70	19 20 32.2	37 44 21.0	99.999	14.722	0.000	0.427
V74	19 21 07.2	37 44 34.9	99.999	14.660	0.000	0.025
V75	19 20 47.9	37 45 58.8	16.829	17.374	0.021	0.053
V79	19 20 55.2	37 46 39.7	18.034	18.631	0.083	0.261
V86	19 20 50.1	37 48 31.7	18.846	19.478	0.134	0.550
V87	19 20 52.8	37 44 58.8	17.637	18.189	0.038	0.094
V90	19 20 58.9	37 44 47.1	17.608	18.159	0.039	0.148
V94	19 20 42.5	37 44 36.9	17.023	17.563	0.034	0.081
V99	19 20 57.1	37 48 12.1	16.866	17.527	0.025	0.045
V114	19 20 00.0	37 48 44.7	16.882	17.601	0.034	0.057

Mochejska, B. J., Stanek, K. Z., Sasselov, D. D., & Szentgyorgyi, A. H. 2002, AJ, 123, 3460 (Paper I)

Monet, D. G., Levine, S. E., Canzian, B. et al. 2003, AJ, 125, 984

Murray, N., & Chaboyer, B. 2002, ApJ, 566, 442

Pinsonneault, M. H., DePoy, D. L., Coffee, M. 2001, ApJ, 556, L59

Santos, N. C., Israelian, G., Mayor, M. 2001, A&A, 373, 1019

Santos, N. C., Israelian, G., & Mayor, M. 2004, A&A, 415, 1153

Seager, S. & Mallén-Ornelas, G. 2003, ApJ, 585, 1038

Stetson, P. B., Bruntt, H., & Grundahl, F. 2003, PASP, 115, 413

Stetson, P. B. 1987, PASP, 99, 191

Street, R. A., et al. 2003, MNRAS, 340, 1287

Udalski, A., Pietrzynski, G., Szymanski, M., Kubiak, M., Zebrun, K., Soszynski, I., Szewczyk, O., & Wyrzykowski, L. 2003, Acta Astronomica, 53, 133

Udalski, A., Szewczyk, O., Zebrun, K., Pietrzynski, G., Szymanski, M., Kubiak, M., Soszynski, I., & Wyrzykowski, L. 2002c, Acta Astronomica, 52, 317

Udalski, A., Zebrun, K., Szymanski, M., Kubiak, M., Soszynski, I., Szewczyk, O., Wyrzykowski, L., & Pietrzynski, G. 2002b, Acta Astronomica, 52, 115

Udalski, A., et al. 2002a, Acta Astronomica, 52, 1

von Braun, K., Lee, B. L., Mallén-Ornelas, G., Yee, H. K. C., Seager, S., & Gladders, M. D. 2004, AIP Conf. Proc. 713: The Search for Other Worlds, 713, 181

Weldrake, D. T. F., Sackett, P. D., Bridges, T. J., & Freeman, K. C. 2005, ApJ, 620, 1043